Enhancing thermoelectric performance via relaxed spin polarization upon magnetic impurity doping

Electronic Supplementary Information

Min Young Kim,[1,a)] Dongwook Kim,[2,a)] Gwansik Kim,[3] Wooyoung Lee,[3,4] Nicolas Perez,[5] Kornelius Nielsch,[5,6,7] Ji Hoon Shim[2,8,b)] and Hyungyu Jin[1,9,b)]

[1]*Department of Mechanical Engineering, Pohang University of Science and Technology (POSTECH), Pohang 37673, South Korea*

[2]*Department of Chemistry, Pohang University of Science and Technology (POSTECH), Pohang 37673, South Korea*

[3]*Department of Materials Science and Engineering, Yonsei University, Seoul 03722, South Korea*

[4]*Affiliate Faculty, Materials Research Center for Batteries, Pohang University of Science and Technology (POSTECH), Pohang 37673, South Korea*

[5]*Leibniz Institute for Solid State and Materials Science, Dresden 01069, Germany*

[6]*Institute of Materials Science, TU Dresden, Dresden 01062, Germany*

[7]*Institute of Applied Physics, TU Dresden, Dresden 01062, Germany*

[8]*Division of Advanced Materials Science, Pohang University of Science and Technology (POSTECH), Pohang 37673, South Korea*

[9]*Adjunct Professor, Institute for Convergence Research and Education in Advanced Technology, Yonsei University, Seoul 03722, South Korea*

[a)] M. Y. Kim and D. Kim contributed equally to this work.

[b)] Authors to whom correspondence should be addressed: jhshim@postech.ac.kr, hgjin@postech.ac.kr

I. Crystal structure of $Mn_{15}Si_{26}$

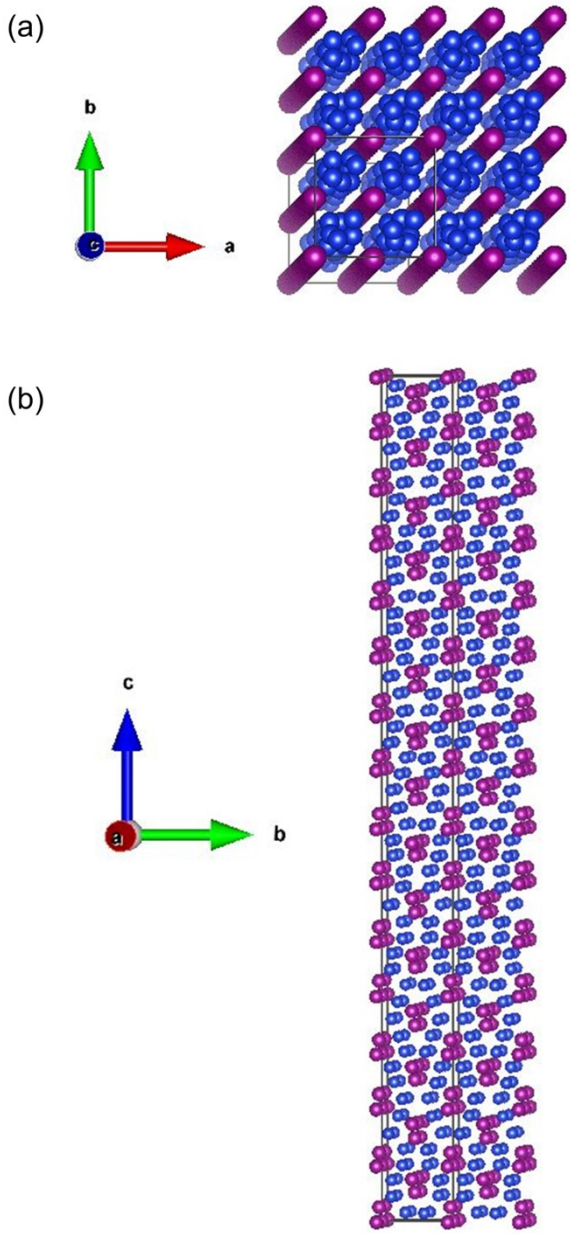

Fig. S1 The unit cells of $Mn_{15}Si_{26}$. (a) Top view: the projection along c-axis. (b) Side view: the projection along b-axis. The pink balls stand for Mn atoms, while the blue balls indicate Si atoms.

Table S1 The crystal structure prediction based on the DFT calculations. The crystal system symmetry, space group and lattice parameters are denoted. Atomic positions for each atom in different Wyckoff positions are listed with type of atom, Wyckoff position and the location in the unit cell.

Crystal system	Space group	a (10^{-10} m)	c (10^{-9} m)	Cell volume (10^{-27} m^3)
Tetragonal	122 (I-42d)	5.49127	6.50445	1.96136
Atom	Wyckoff position	x/a	y/b	z/c
Mn1	4a	0	0.5	0.25
Mn2	8c	0.5	0	0.215239
Mn3	8c	0.5	0	0.151095
Mn4	8c	0.5	0	0.081816
Mn5	8c	0.5	0	0.017338
Mn6	8c	0	0.5	0.448819
Mn7	8c	0	0.5	0.383626
Mn8	8d	0	0.5	0.316227
Si1	16e	0.346528	0.250000	0.125000
Si2	16e	0.153516	0.288455	0.354444
Si3	16e	0.315266	0.656436	0.335354
Si4	16e	0.337199	0.167973	0.317052
Si5	16e	0.159092	0.824680	0.298819
Si6	16e	0.770175	0.653452	0.010401
Si7	16e	0.154471	0.803174	0.030268

II. Magnetic field H dependence of Hall resistivity ρ_{xy}

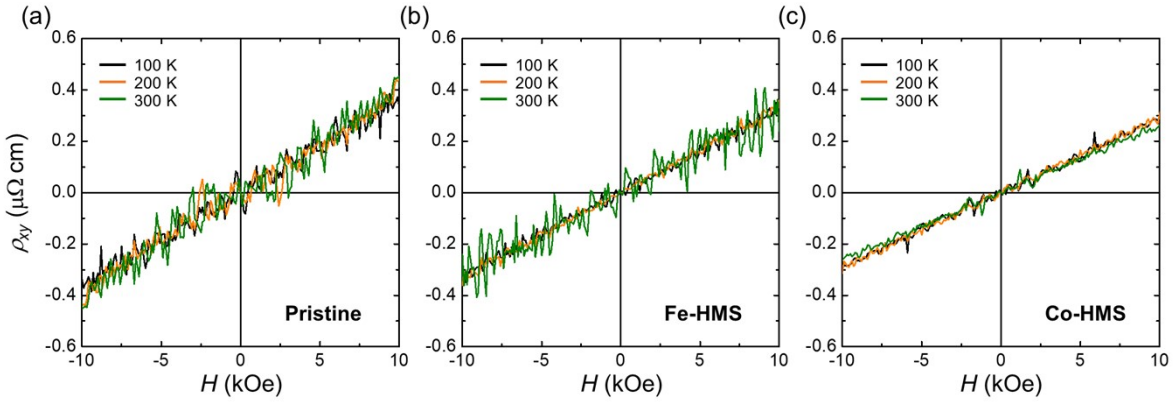

Fig. S2 Magnetic field H dependence of Hall resistivity ρ_{xy} of pristine, Fe-HMS and Co-HMS samples at 100, 200 and 300 K.

III. Crystal structure analysis using powder X-ray diffraction

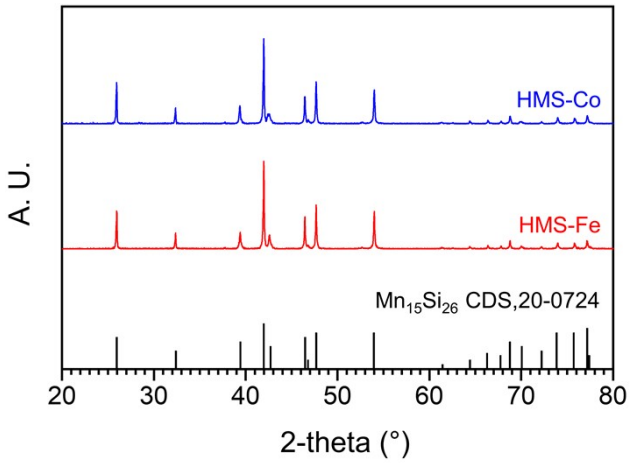

Fig. S3 Powder X-ray diffraction (XRD) patterns of Fe-HMS and Co-HMS after the fabrication process.

Table S2 *a*-axis and *c*-axis lattice constants *a* and *c* of pristine, Fe-HMS and Co-HMS.

	a (Å)	*c* (Å)	Cell volume (10^{-27} m^3)	Deviation (%)
Pristine	5.523	65.41	2.00	+1.02 %
Fe-HMS	5.519	65.29	1.99	+1.01 %
Co-HMS	5.516	65.36	1.99	+1.02 %

IV. Microstructure analysis using scanning electron microscope imaging

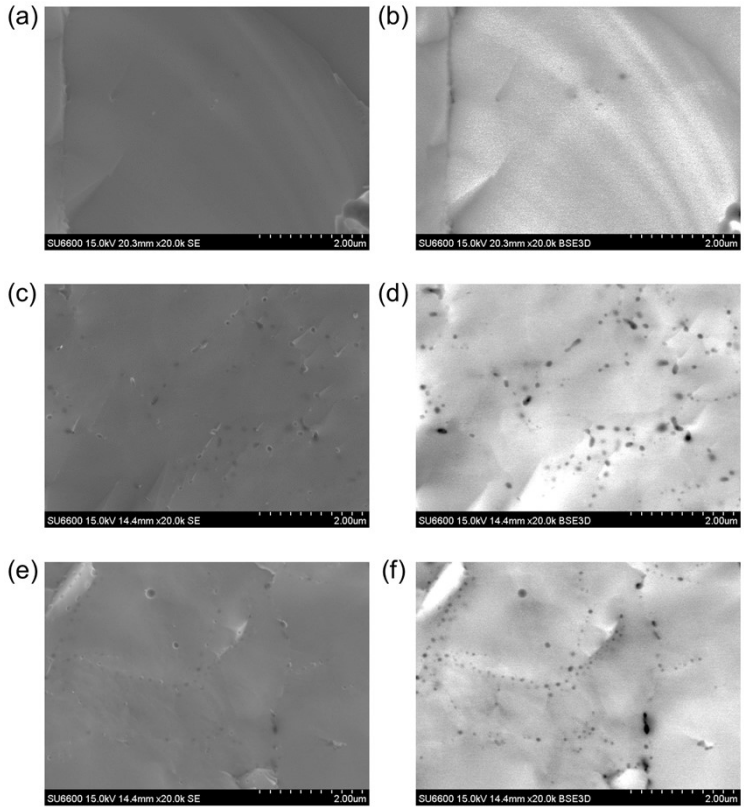

Fig. S4 (Left) secondary electron (SE) and (right) back-scattered electron (BSE) images of (a),(b) pristine, (c),(d) Fe-HMS and (e),(f) Co-HMS.

V. Spin-polarized band structures of $Mn_{15}Si_{26}$ with different magnetic moments

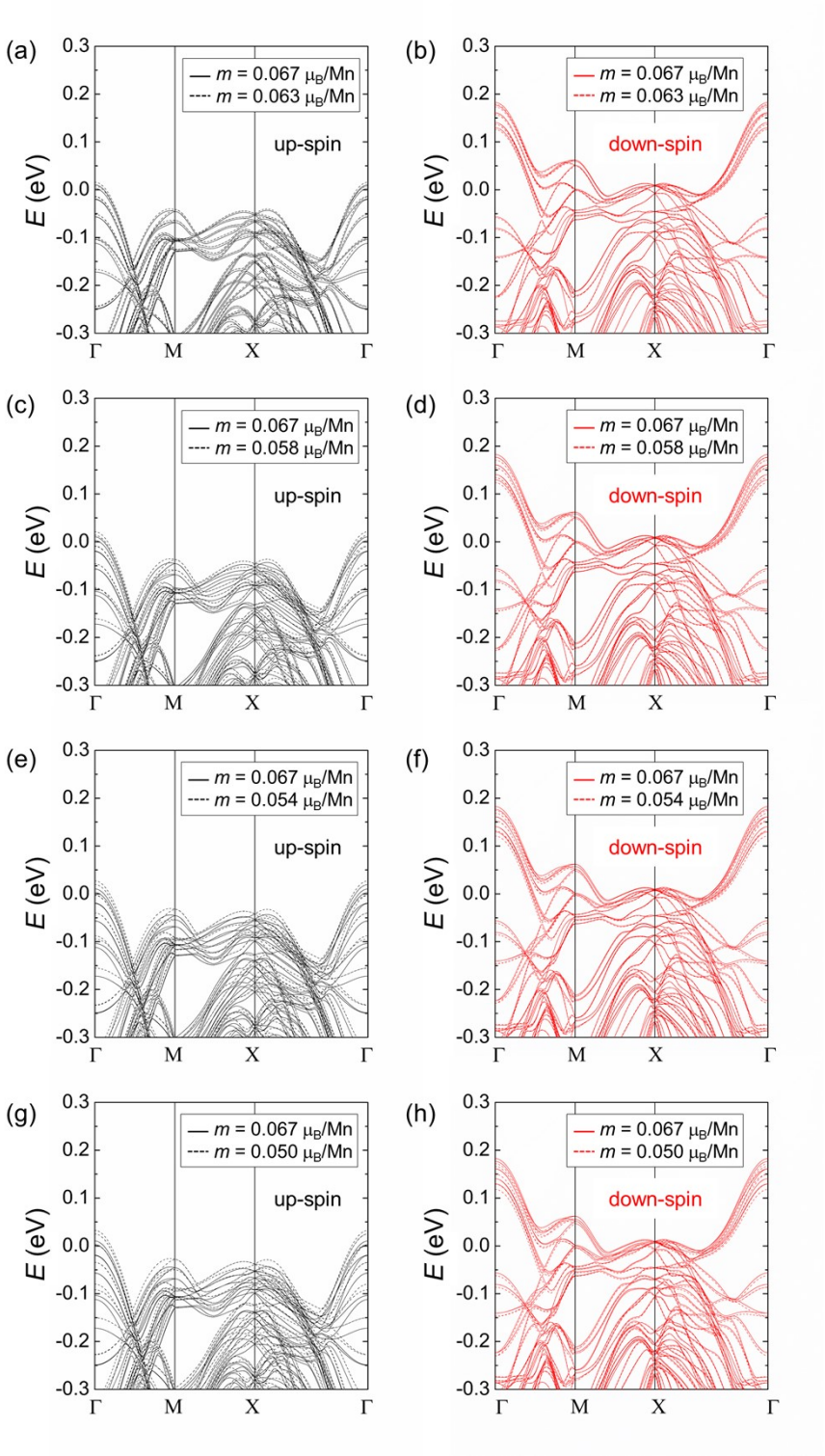

Fig. S5 Comparison of up-spin and down-spin band structures between the pristine (m = 0.067 μ_B/Mn) and magnetically doped cases with various magnetic moments of (a-b) m = 0.063 μ_B/Mn, (c-d) m = 0.058 μ_B/Mn, (e-f) m = 0.054 μ_B/Mn and (g-h) m = 0.050 μ_B/Mn. The

black and red lines correspond to the up-spin and down-spin bands, respectively. The solid and dotted lines correspond to m = 0.067 μ_B/Mn and m = 0.063 to 0.050 μ_B/Mn, respectively.

VI. Temperature dependence of lattice thermal conductivity κ_L

The lattice contribution to the total thermal conductivity κ can be estimated using the Wiedemann-Franz law of $\kappa_{ele} = L\sigma T$ (κ_{ele}: electron thermal conductivity, σ: electrical conductivity and L: the Lorentz number). The lattice thermal conductivity κ_L is the difference between κ and κ_{ele}, which is shown in **Fig. S5**.

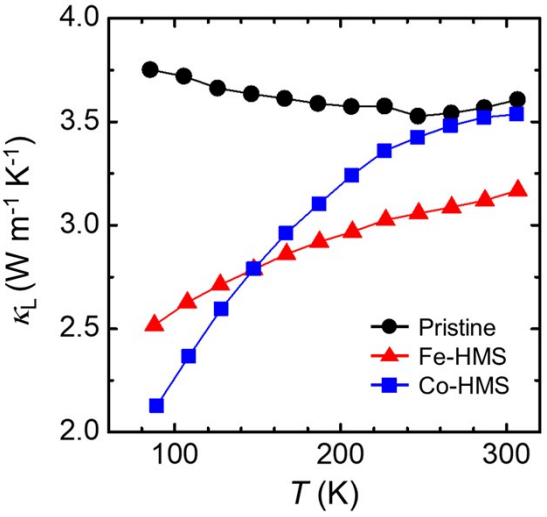

Fig. S6 Temperature T dependence of lattice thermal conductivity κ_L of pristine, Fe-HMS and Co-HMS. -●-: Pristine HMS, -▲-: Fe-HMS and -■-: Co-HMS.

VII. A curve fitting for estimating density-of-states (DOS) effective mass

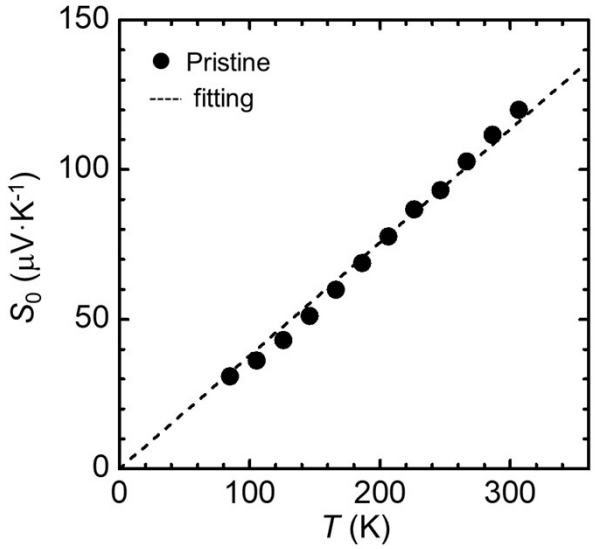

Fig. S7 (a) The linear fitting of Seebeck coefficient of the pristine S_0 for the estimation of density-of-states (DOS) effective mass m_{D}^{*} of the pristine sample. The black dashed line is fitting line for the prediction of m_{D}^{*}.

VIII. Spin-polarized density functional theory calculation results of $Mn_{15}Si_{26}$ phase

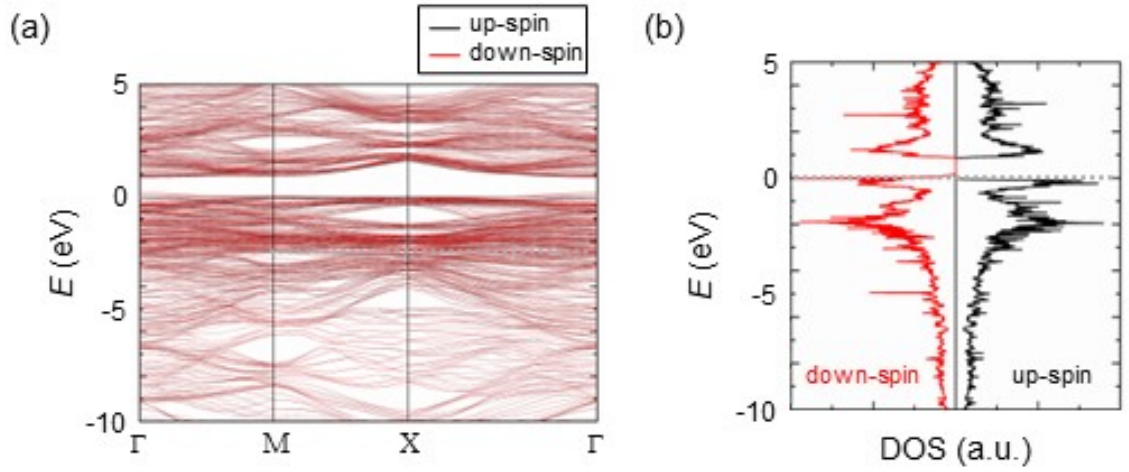

Fig. S8 (a) The spin-dependent band structures and (b) density-of-states (DOS) of up- and down-spin bands of $Mn_{15}Si_{26}$ at a broad range of E (-10 eV < E < 5 eV).